[0001] Oriented Aluminum Nitride One-Dimensional Nanostructures: Synthesis, Structure Evolution, and Electrical Properties

Jie Zheng,[†] Yuan Yang,[‡,∥] Bo Yu,[†] Xubo Song,[†] and Xingguo Li[†,§,*]

[†]Beijing National Laboratory for Molecular Sciences (BNLMS) (The State Key Laboratory of Rare Earth Materials Chemistry and Applications), College of Chemistry and Molecular Engineering, Peking University, Beijing 100871, P. R. China, [‡]Electron Microscopy Laboratory and State Key Laboratory for Mesoscopic Physics, College of Physics, Peking University, Beijing 100871, China, [§]College of Engineering, Peking University, Beijing 100871, P. R. China. [∥]Current Address: Department of Materials Science and Engineering, Stanford University, California 94305.

Downloaded via COLUMBIA UNIV on August 21, 2018 at 21:06:01 (UTC).
See https://pubs.acs.org/sharingguidelines for options on how to legitimately share published articles.

ABSTRACT This paper presents a systematic investigation on the controlled synthesis of wurtzite aluminum nitride (AlN) one-dimensional (1D) nanostructures in a chemical vapor deposition (CVD) system using Al and NH_3 as starting materials. By controlling reaction temperature and NH_3 flow, nanostructures with manifold morphologies including nanoneedles, branched nanoneedles, short nanorods, slim nanorods, and nanofences were synthesized with high yield and selectivity. The correlation between experiment parameters and product morphologies was interpreted by a surface diffusion based model. Moreover, electrical properties of a single nanoneedle were studied for the first time, in which typical semiconductor characteristics were observed. Silicon was speculated to incorporate into the AlN nanoneedle from silicon substrates during the synthesis, which served as an *n*-type donor and was responsible for the observed electrical behavior.

KEYWORDS: Aluminum nitride · one-dimensional nanostructures · controlled synthesis · electrical properties

Aluminum nitride is an important functional material for electronics and optoelectronics. It has the largest band gap in group III nitrides, which makes it an essential material when pursuing even shorter wavelength of light emission devices.[1] It is also attractive for field emission applications because of its low electron affinity and thermal stability.[2] Other important applications of AlN include surface acoustic wave devices[3] and buffer layers for group III nitride thin film epitaxy.[4] In addition, AlN is desirable for its chemical and thermal stability, mechanical strength, and compatibility to silicon and other group III nitrides, which makes it adaptable to a large variety of environments and enables large freedom in its device fabrication. The growth of AlN bulk crystals and thin films has received attention for a long time. Recently, one-dimensional (1D) nanostructures have attracted intense research interest because of their unique physical properties and potential applications as building blocks in nanoscale electronics.[5] Consequently, large efforts have been devoted to the synthesis of 1D AlN nanostructures in pursuing improved physical properties. On the basis of the chemical vapor deposition (CVD) technique using Al/NH_3 or $AlCl_3$/NH_3 as starting materials, a large variety of 1D AlN nanostructures including nanowires[6] nanobelts,[7,8] nanoneedles,[9–11] and nanotubes[12] were prepared. Indeed, significantly enhanced field emission properties were observed in 1D AlN nanostructures with large curvature geometries.[13–17]

To achieve precise morphology control, it is critical to understand the relationship between product morphologies and experimental parameters such as temperature and gas flow. However, this is still a rarely explored field at present. In this article, we demonstrate that by controlling temperature and NH_3 flow, 1D AlN nanostructures with manifold morphologies could be selectively prepared in an Al/NH_3 CVD system. All of the obtained nanostructures were [0001] oriented. The mechanism for structure evolution with temperature and NH_3 flow was discussed on the basis of a surface diffusion model.

A knowledge of the electrical properties of AlN 1D nanostructures is the first step to realizing their application in electronic/optoelectronic nanodevices. However, the electrical properties of 1D AlN nanostructures have not been reported yet. In this article, the electrical properties of a single nanoneedle were studied for the first time,

*Address correspondence to xgli@pku.edu.cn.

Received for review August 5, 2007 and accepted December 17, 2007.

Published online January 5, 2008.
10.1021/nn700363t CCC: $40.75

© 2008 American Chemical Society

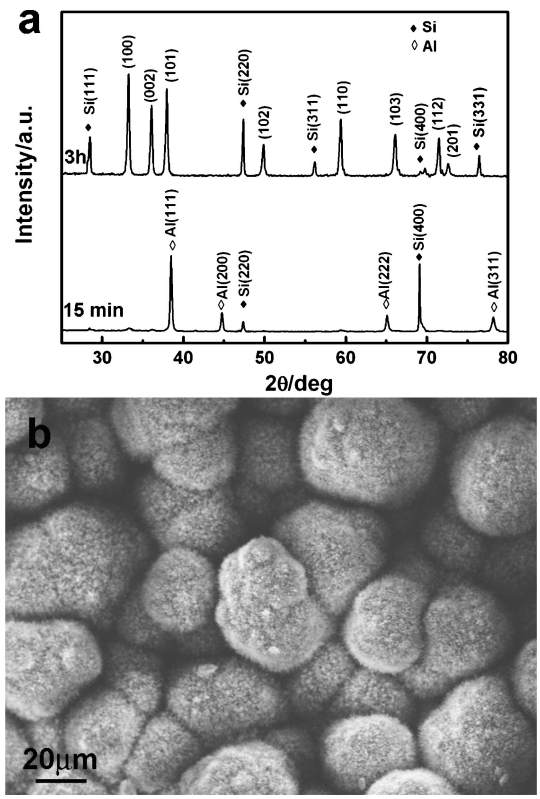

Figure 1. (a) Typical XRD patterns of the obtained AlN nanostructures after deposition for 15 min (lower curve) and 3 h (upper curve). The solid and hollow rhombs indicate the diffraction peaks from silicon (JCPDS 27-1402) and aluminum (JCPDS 04-0787), respectively. (b) A typical low magnification SEM image showing the spherical aggregation of the AlN 1D nanostructures. The sample was prepared at 950 °C and 1 sccm NH_3 on the upper side. The products obtained by other temperature−NH_3 flow combinations exhibited similar characteristics.

in which typical semiconductor characteristics were observed. The incorporated Si from the Si substrates served as an *n*-type donor and was responsible for the observed electrical behavior.

RESULTS AND DISCUSSION

An Overview of the Growth. All of the products obtained were wurtzite AlN (JCPDS 25-1133) as confirmed by the XRD results (Figure 1a, upper curve). No significant peak shift or broadening was observed when temperature and NH_3 flow changed in our experiment series. Notably, polycrystalline Si diffraction peaks (JCPDS 27-1402) with remarkable intensity were detected in all cases, as indicated by the solid rhombs. The XRD pattern of the single crystalline Si (100) substrates consisted of only a sharp peak at 69° corresponding to the (400) diffraction. The polycrystalline type diffraction pattern suggests that the silicon substrates were also involved in the reaction. The reaction of Si substrates in the growth of AlN nanostructures has been observed previously in the case of AlN nanoneedles.[14] However, the reason was not discussed in detail. In the beginning of growth when the Al supply succeeded NH_3 flow, excessive Al was deposited on the substrates (Figure 1a, lower curve). Since the reaction temperature was high above the Al melting point, the unconverted Al was in liquid form. Liquid Al was able to etch some part of the silicon substrates because of the tendency to form Al−Si alloy. However, the existence of separated Al and Si phases in the initial deposition stage (Figure 1a, lower curve) suggested that Si was only dissolved in liquid Al without forming a homogeneous alloy phase. During the nitridation process, Al was converted to AlN, and Si precipitated as a separated phase in the polycrystalline form. A certain amount of silicon was able to enter the AlN lattices during the growth process, which was critical for the electrical properties of the AlN 1D nanostructure, as discussed in the electrical property measurement section.

The liquid Al in the initial growth stage also led to the aggregation of obtained nanostructures into spherical islands about several tens of microns in size (Figure 1b). This phenomenon was always observed for the deposition on the upper side of the substrates. On the lower side, the deposition amount was smaller, and the aggregation phenomenon was inappreciable. Since almost all of the samples were collected on the upper side with only one exception, we focus on the growth on the upper side here and will discuss the growth on the lower side in the corresponding section. The spherical aggregation resulted from the condensed liquid Al, which suggested that the nucleation of the AlN nanostructures on the upper side should take place from liquid Al. Because of this reason, the morphologies of the AlN nanostructures showed little dependence on substrate conditions. A more detailed discussion on the effects of silicon substrates can be found in the Supporting Information.

Despite the existence of liquid metal, the growth of AlN 1D nanostructures was unlikely to follow the vapor–liquid–solid (VLS) mechanism. In the VLS mechanism, a liquid nanoparticle is present in the growth frontier of each 1D nanostructure to receive the gas phase precursor and guide nanostructure growth.[5] In our experiments, AlN nanostrutures with six different morphologies were obtained under different temperature−NH_3 flow combinations, as shown in Figure 2. All of the nanostructures were absent of silicon-containing nanoparticles or nanoparticles from condensed melts in the tip part, which excluded the VLS mechanism because of the catalytic effect of the Al−Si alloy or Al self-catalysis. Therefore, we concluded that the growth mechanism of our AlN nanostructures was the Vapor−Solid (VS) mechanism, in agreement with those reported in literature.[11]

In typical VS growth processes, the incorporation of gaseous species into the solid phase involves the following steps: the incidence of gaseous species onto the solid surface and surface diffusion and capture of the diffusion species by certain sites on the solid surface. Therefore, we speculated that the change of surface dif-

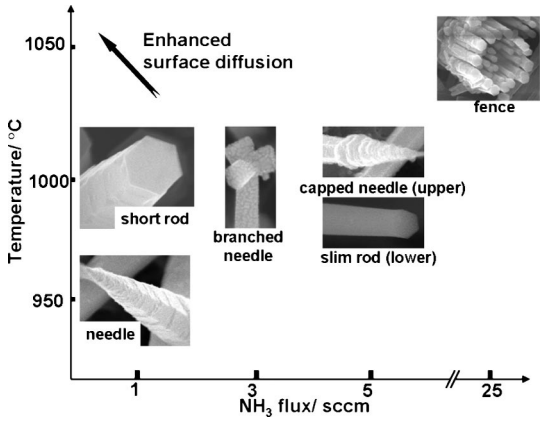

Figure 2. AlN nanostructures obtained under different temperature−NH_3 flow combinations.

fusion conditions at different temperatures and NH_3 flow was responsible for the structure evolution. Surface diffusion is enhanced at higher temperature because higher temperature is beneficial for overcoming the diffusion energy barriers. Also, higher Al/N ratio in the ambience facilitates surface diffusion, especially on the (0001) surfaces. The AlN (0001) surfaces are always Al-terminated.[18] In the Al-rich condition, weak, delocalized Al−Al bonds were formed on the surface, which could serve as a lubricant. In contrast, excessive nitrogen species in the ambience results in the formation of strong, covalent Al−N bonds, which suppress surface diffusion. In our system, in addition to the pure temperature effect, higher temperature also enhanced surface diffusion by accelerating Al evaporation to create a more Al-rich ambience. Surface diffusion conditions shape the growth behaviors of nanostructures to a great extent. Large area smooth surfaces tend to form when surface diffusion is enhanced. However, suppression of surface diffusion usually results in surface roughing and island formation. These phenomena were observed extensively in AlN,[19] GaN,[20] and InN[21] thin film epitaxy and their nanostructure growth.[22−24] In the following sections, we will demonstrate how these principles interpret the evolution mechanism of different AlN nanostructures.

Characterization of Product Morphologies and Mechanism for Structure Evolution. ***Nanoneedles.*** The product collected on the upper side of Si substrates at 950 °C with 1 sccm NH_3 was nanoneedles (Figure 3a). The nanoneedles were typically 200 to 300 nm in diameter at the bottom and with sharp tips around 10 nm. The length of the nanoneedles could reach 10 μm (Figure 3c). Close inspections revealed that the nanoneedles had hexagonal cross sections and layer-stacked structure along the growth direction (Figure 3b). Figure 3d presents a typical TEM image of a single nanoneedle and the corresponding electron diffraction pattern. The electron beam irradiated along the [2 $\bar{1}$ $\bar{1}$ 0] direction, and the growth direction was [0001]. The distance of neighboring lattice fringes was 0.249 nm (Figure 3e and Figure 3f), corresponding to that of (0002) planes of wurtzite AlN. This result is consistent with the hexagonal cross section observed in SEM images. The EDS measurement

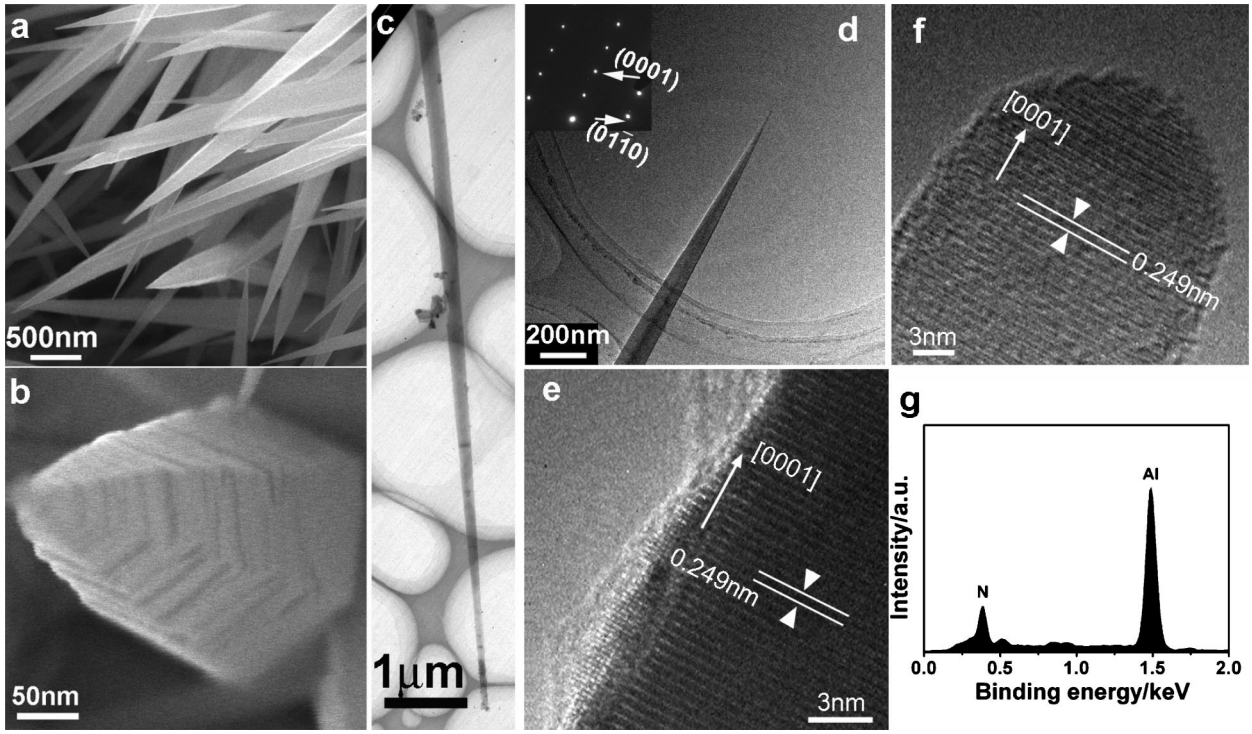

Figure 3. (a and b) SEM images with different magnifications of AlN nanoneedles. (c) A full length TEM image. (d) A TEM image. Inset: the corresponding electron diffraction pattern. (e) The HRTEM image of the stem. (f) The HRTEM image of the tip part. (g) The EDS spectrum. The product was collected on the upper side of substrates at 950 °C and 1 sccm NH_3.

of a single AlN nanoneedle indicated that the nanoneedle was composed of Al and N, with negligible silicon content (Figure 3g).

The structure of the nanoneedles could be described as the layer-by-layer stacking of hexagonal platelets with gradually shrinking size along the [0001] direction. The shrinkage of platelet size was a result of an energy barrier (the Ehrlich−Schwoebel barrier), which prevented the adatoms hopping down steps to preserve steps.[25,26] The AlN nanotips reported by Shi et al.[11,22] were very similar in morphology and growth behavior except the much smaller length (typically 1–2 μm) of their samples. In fact, both the bottom diameter and length of our samples were 3–4 times larger than those of theirs. The geometric resemblance between the two samples suggests that their growth was governed by similar mechanisms. The larger length of our nanoneedles was a result of the larger basal plane formed at the nucleation stage. Both short and long nanoneedles were obtained at nearly identical temperature (950 °C). However, the NH_3 flow in our synthesis was much lower. According to the previous discussion, a larger Al/NH_3 ratio was favorable for the formation of large, smooth (0001) surfaces. Therefore, the initially formed hexagonal platelets, which served as the nuclei, were expected to be larger at higher Al/NH_3 ratios, which assured a larger length of the nanoneedles, provided that the contraction rate of platelet size were the same in the two cases.

Short Nanorods. Raising the reaction temperature to 1000 °C at the same NH_3 flow (1 sccm) and collection position flattened out the tips of nanoneedles and resulted in the formation of nanorods. (Figure 4). Compared to the nanoneedles, the nanorods are larger in diameter (400 nm) but shorter in length (1–2 μm). Hexagonal cross sections and layer-stacked structure are also observed here (Figure 4c, Figure 4d), suggesting their structural similarity with the nanoneedles. The evolution from nanoneedles to nanorods was ascribed to the enhanced surface diffusion at elevated temperature. This observation was in agreement with that reported by Shi et al.,[22] where a detailed discussion can be found.

Branched Nanoneedles. When NH_3 flow increased at 1000 °C, branches appeared at the tips of the nanoneedles (1000 °C; 3 sccm NH_3 flow, collected on the upper side of substrate; Figure 5). The stems were in close resemblance to that of the nanoneedles except for the smaller length and diameter, which originated from a smaller Al/NH_3 ratio as discussed above. The growth direction of the stem is along the [0001] direction, as indicated by electron diffraction, HRTEM, and their hexagonal cross section (Figure 5f and Figure 5g). The branches were short nanowires about 100 to 200 nm in length. The exact growth directions of the branches could not be determined by HRTEM because of technical difficulties. However, their hexagonal cross sections suggested that

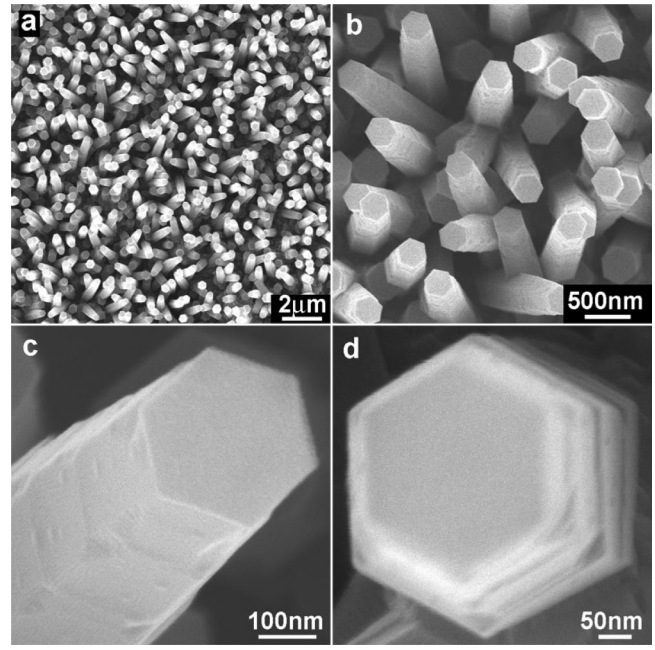

Figure 4. SEM images with different magnifications of AlN nanorods. The product was collected on the upper side of substrates at 1000 °C and 1 sccm NH_3.

they also grew along the [0001] direction (Figure 5b and Figure 5c).

The formation of branched nanoneedles can be viewed as the attachment of smaller hexagonal prisms to the stem. Most branched nanoneedls have three symmetrically distributed branches that attached to the stem in generally two modes, as illustrated in Figure 5d and Figure 5e. In mode 1, each branch attached to the stem through two adjacent side walls of the stem hexagonal prism (Figure 5d). In mode 2, one of the six side walls and two halves of its two neighboring side walls were used for branch attachment (Figure 5e). Therefore, the growth of branches was a result of secondary growth on the six side walls, which were $\{1\bar{1}00\}$ facets of the stem. The branching sites were at the tip part, indicating that secondary growth was not initiated until certain duration of the nanoneedle growth. With the progress of the reaction, the Al/NH_3 ratio gradually decreased because aluminum was consumed, which caused surface roughing. From the high magnification SEM images (Figure 5b and Figure 5c), the tip parts of the branched nanoneedles were very rough and covered with many small nanocrystals. Defective structures were also observed in the HRTEM image (Figure 5g). The rough and defective surface provided nucleation sites for the nucleation on the $\{1\bar{1}00\}$ facets and the subsequent growth of the short branches.

Although nanoneedles with three branches were most frequently observed, the number of branches could vary from 2 to 4. The configuration of the branches could also be different with the same branch number (see Supporting Information, Figure S2). No

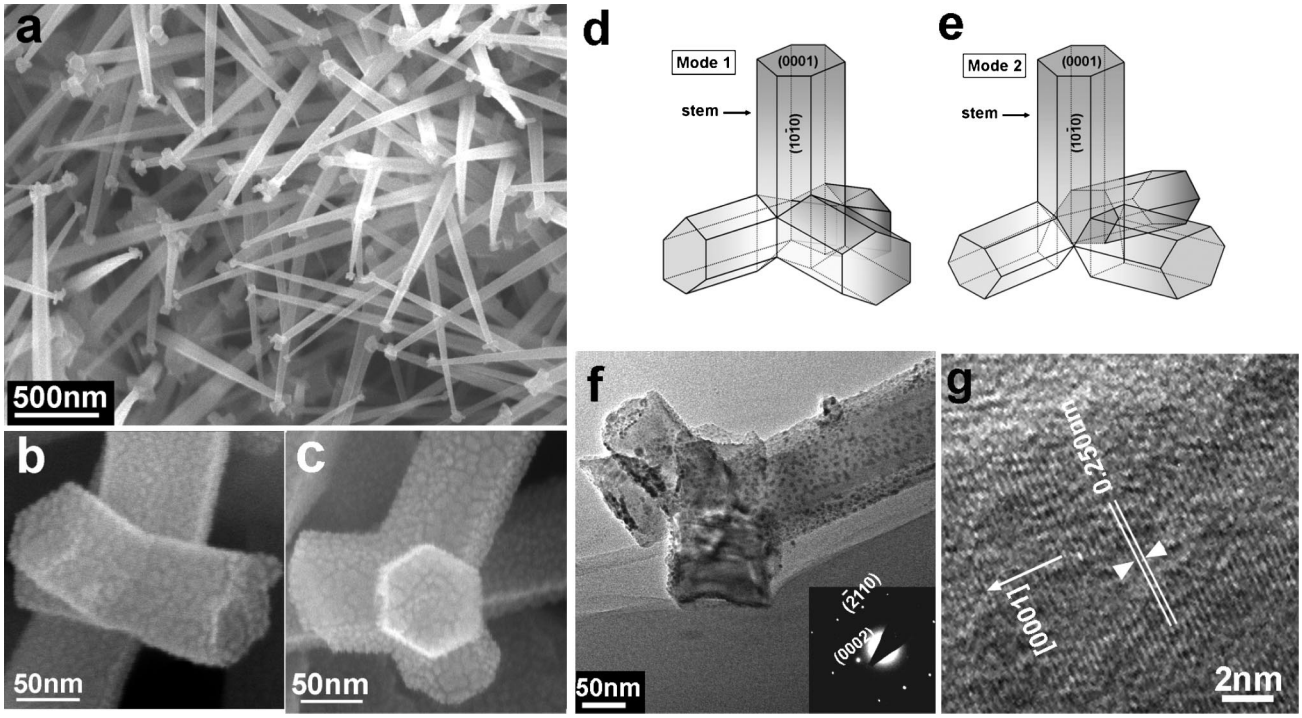

Figure 5. (a, b, and c) SEM images of AlN branched nanoneedles. (d and e) illustration of the corresponding attach modes in (b) and (c), respectively. (f) A TEM image of a branched nanoneedle; inset, the corresponding electron diffraction pattern. (g) The HRTEM image of the branched nanoneedle. The product was collected on the upper side of substrates at 1000 °C and 3 sccm NH_3.

specific crystallographic orientation of the branches with respect to the stem was observed.

Capped Nanoneedles. Another derivative of the nanoneedles was obtained if we further increased the NH_3 flow to 5 sccm at 1000 °C, as shown in Figure 6. The product maintained the hexagonal needle-like profile, but with a cone capped on their tips. Although the caps were rough and irregular in shape, they showed a certain degree of epitaxial growth on the hexagonal nanoneedles (Figure 6d). The rough cap could also be ascribed to the surface roughening effect of even reduced Al/NH_3 ratio after certain duration of growth.

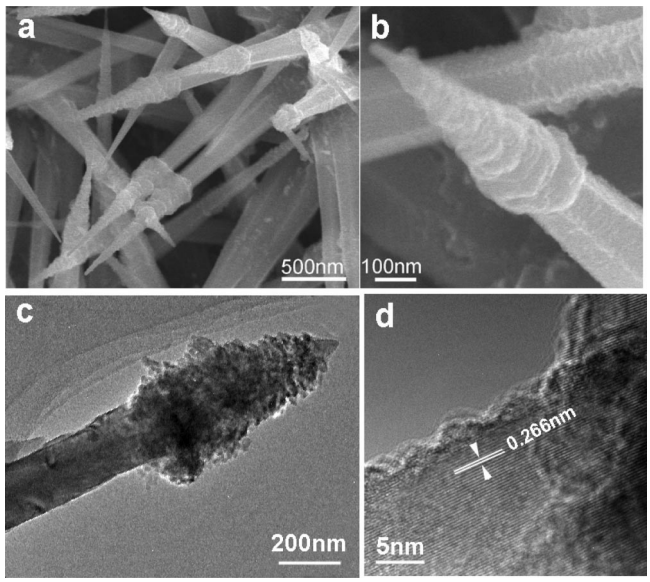

Figure 6. (a and b) SEM images of capped AlN nanoneedles. (c and d) TEM and HRTEM images of a capped needle. The product was collected on the upper side of substrates at 1000 °C and 5 sccm NH_3.

Slim Nanorods. The product collected on the lower side of substrates at 1000 °C with an NH_3 flow of 5 sccm were slim nanorods (Figure 7). The nanorods were typically 200 nm in basal plane diameter and over 10 μm in length. The diameter of the growth frontier was smaller than the basal plane, but the contraction rate was much slower compared to that of the nanoneedles. The growth direction of the slim nanorods was also [0001], as confirmed by electron diffraction and HRTEM (Figure 7c and Figure 7d). However, the hexagonal cross sections were not clear and the layer-stacked structure was not observed (Figure 7b, inset). Compared to the capped nanoneedles collected on the upper side, the slim nanorods were smaller in diameter but larger in length. The growth ambience on the lower side was Al-richer compared to that of the upper side at the same experimental parameters because the lower side faced the Al powder directly. Therefore, surface diffusion was more favorable on the lower side. As shown in the nanoneedle-to-nanorod transition, enhanced surface diffusion helped surface atoms overcome the energy barrier, which alleviated step formation and diameter contraction. As a result, the slim nanorods exhibited a slower diameter shrinkage rate, larger final length, and smoother surface compared to those of the capped nanoneedles collected on the opposite side of the substrates.

Nevertheless, the diameter of the slim nanorods was smaller than the capped nanoneedles, which could

not be explained by the diffusion-based mechanism alone since larger nuclei were expected for surface diffusion-favorable ambience. The complexity arose from the difference in the initial growth stage on the upper and lower sides of the substrates. As discussed above, the nanostructures on the upper side were nucleated from liquid Al. The average size of the Al liquid drops was several tens of microns, a scale indicating that gravity still mattered. As a result, the lower side was hardly able to hold the Al liquid. Thus, the nucleation on the lower side was likely to be a standard VS process, that is, direct condensation from the gas phase, which was expected to yield smaller nucleus size compared to the nucleation from liquid due to the deficiency in materials. However, when the VS mechanism took charge of the growth process after the nucleation stage, the diffusion-based model worked well for the different morphologies of the products on the upper and lower sides.

Nanofences. A hierarchical structure was obtained under 1050 °C with an NH_3 flow of 25 sccm on the upper side (Figure 8). Many short hexagonal prisms about 50 nm in diameter (Figure 8a, inset) were aligned in parallel along the periphery of the hexagonal surface of a larger hexagonal prism, building up a fence-like structure (Figure 8b). The growth direction of small hexagonal prisms was the [0001] direction, as confirmed by the HRTEM image (Figure 8d). The SEM image shows that all of the short hexagonal prisms attached to the (0001) surface of the large hexagonal prism via their hexagonal surfaces. Therefore, their orientations were nearly identical, as indicated in the electron diffraction pattern (Figure 8c, inset). The bright spots were composed of several smaller spots, which could be attributed to the slight divergence of the small hexagonal prism orientations.

The growth of the small hexagonal prisms was initiated by the nucleation on the (0001) surface of the large hexagonal prism. The large base hexagonal prism was formed because of higher temperature, which enhanced diffusion length. The nucleation and subsequent growth of short nanorods resulted from the reduced Al/NH_3 ratio as growth proceeded. Interestingly, the density of nanorods along the periphery was much higher than that in the middle part of the hexagonal plane. Steps and kinks on the surface are most capable of capturing surface diffusion species, resulting in higher nucleation probability in these sites. Therefore, secondary growth was more likely to take place in the periphery of the large hexagon where the density of steps and kinks was higher. A similar phenomenon was observed in the noncatalytic growth of ZnO nanotubes.[27]

All the nanostructures discussed above were based on [0001] oriented 1D structures and could be structurally regarded as derivatives of a hexagonal prism prototype. Both temperature and NH_3 flow shaped the product morphologies by changing the surface diffusion conditions. As a general trend, surface roughening and secondary growth were favored when surface diffusion was suppressed (lower Al/NH_3 ratios and lower temperature), while smooth surfaces tended to be formed when surface diffusion was enhanced (higher Al/NH_3 ratios and higher temperature).When the temperature

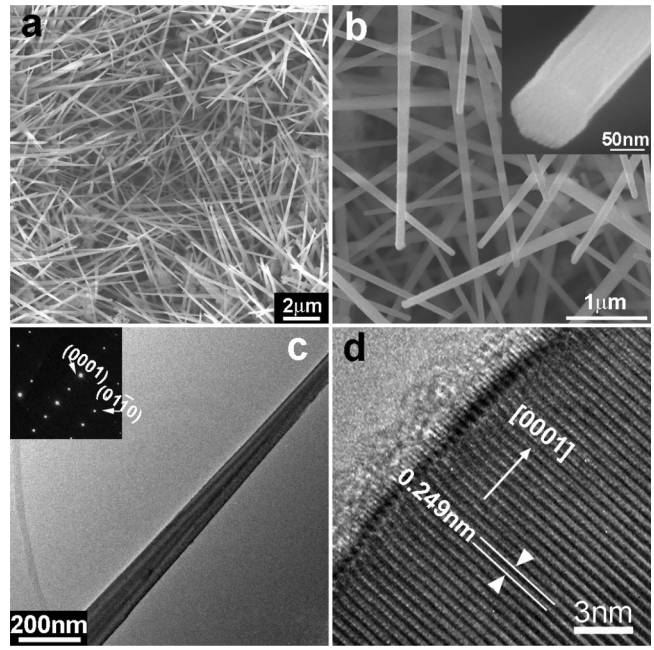

Figure 7. (a and b) SEM images of AlN slim nanorods. Inset in (b): a high magnification SEM image of the tip part of a slim nanorod. (c) A TEM image. Inset in (c): the corresponding electron diffraction pattern. (d) The HRTEM image. The product was collected on the lower side of substrates at 1000 °C and 3 sccm NH_3.

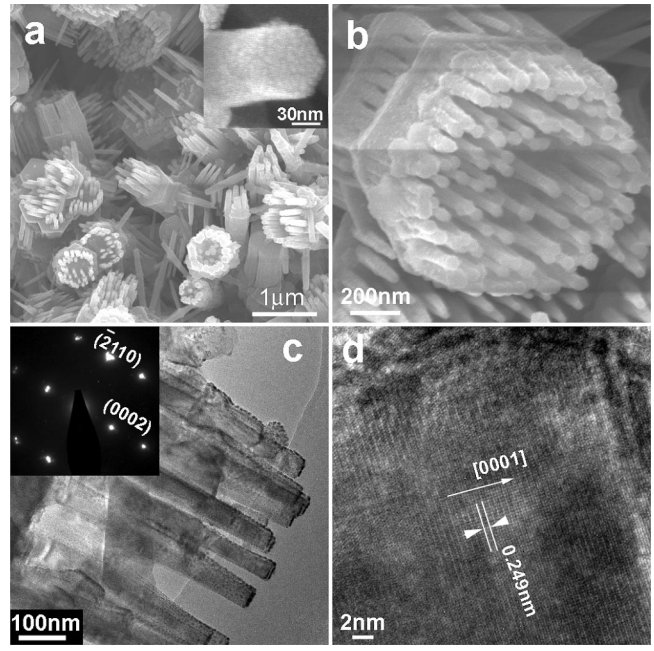

Figure 8. (a and b) SEM images of AlN nanofences. Inset in (a): a high magnification SEM image of a nanorod making up the nanofence. (c) A TEM image. Inset in (c): the corresponding electron diffraction pattern. (d) The HRTEM image.

and NH_3 flow increased simultaneously, their effects were contradictory. In our experiments, NH_3 flow seemed to be a more influential factor that usually compensated the effect of temperature increase. For example, the branched nanoneedles obtained at 1000 °C and 3 sccm NH_3 were smaller in diameter than the nanoneedles obtained at 950 °C and 1 sccm, which originated from the increased NH_3 flow, because the increased temperature was supposed to enlarge the nanoneedle diameters, as that observed in the short nanorods obtained at 1000 °C and 1 sccm NH_3. The importance of the NH_3 flow effect was because most growth processes were carried out at low NH_3 flows and a slight change in NH_3 flow would cause significant variation of Al/NH_3 ratios. Especially, with the consumption of Al along the reaction process, the Al/NH_3 ratio was reduced, which usually caused surface roughening and secondary growth after a certain duration of growth. With the above guidelines, the mechanism for the product morphology evolution with the experimental parameters could be understood. The conclusions obtained here may provide insight into the morphology control and design of other AlN 1D nanostructures.

Electrical Property Measurement. As the first step toward AlN-based electronic/optoelectronic nanodevices, we studied the electrical properties of AlN nanoneedles. First, AlN nanoneedles were dispersed on sapphire substrates. Then the contacts were formed by evaporation of Ti (10 nm)/Au (90 nm) electrodes and fixed by depositing Pt through a focused ion beam. Current–voltage (I-V) characteristics were measured at 5×10^{-5} Torr from 180 to 300 K with a step of 30 K. An SEM image of the whole device is shown in the inset of Figure 9a. Five different nanoneedles were measured.

Figure 9a shows typical I-V curves of a single nanoneedle sample from 180 to 300 K. The electrical conductance of the nanoneedle increased with temperature, which was typical semiconductor behavior. All curves showed slight nonlinearity, especially those measured at low temperatures, which was likely to result from the Schottky barriers at the two contacts. In order to minimize the influence of the Schottky barrier, only the high voltage bias data (>5 V) were selected to calculate the conductivity. Using geometric parameters (diameter of the two ends, 220 and 300 nm, respectively; effective length, 3.0 μm.), the electrical conductivity of the nanoneedle (σ) was calculated to be $8 \times 10^{-6}\ \Omega^{-1}\ cm^{-1}$. The conductivity of the other nanoneedles was of the same order.

The band gap of AlN is 6.2 eV. Therefore, band edge excitation can be neglected at room temperature. The carriers primarily originated from the excitation of impurities, which were most likely to be Si and O in our experiment, from the silicon substrates and residue oxygen, respectively. According to previous reports, oxygen usually forms deep levels in AlN;[28,29] therefore, it is unlikely to result in the measured conductivity.

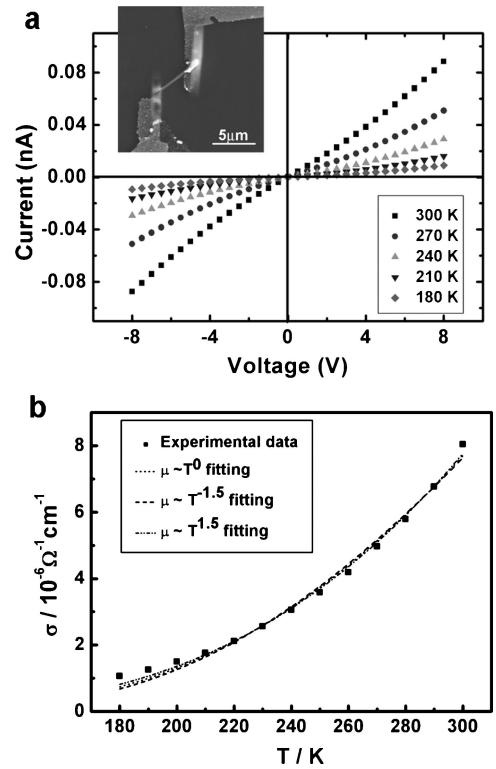

Figure 9. (a) Current–voltage characteristics of a single AlN nanoneedle measured from 180 to 300 K with a step of 30 K; inset, an SEM image of the device fabricated for electron conductance measurement of an AlN nanoneedle. (b) The temperature dependence of conductivity of the AlN nanoneedle. The dot-dashed and dash-dotted lines correspond to the fitted function using equations listed in Table 1.

However, silicon usually serves as an *n*-type donor in AlN with excitation energy around 200 to 300 meV.[30–32] To determine the impurity contributing to the conductivity, the ionization energy (E_i) of the impurity was estimated from the temperature dependence of the conductivity.

The conductivity (σ) of a nanoneedle was expressed in eq 1 as follows:[33]

$$\sigma = e\mu n = e\mu\left(\frac{N_C N_D}{2}\right)^{1/2} \exp\left(-\frac{E_i}{2k_B T}\right) \qquad (1)$$

where e is the charge of an electron, n is the carrier concentration, μ is the electron mobility, E_i is the activation energy, k_B is the Boltzmann's constant, N_D is the dopant concentration, and N_C is the effective density of states. The expression for N_C is described in eq 2 as follows:

TABLE 1. Activation Energy Values for Different Scattering Mechanisms

scattering mechanism	$\sigma - T$	fitted E_i (meV)
acoustic	$\sigma \propto T^{-0.75}\exp(-E_i/2k_BT)$	218±5
Coulomb	$\sigma \propto T^{2.25}\exp(-E_i/2k_BT)$	86 ±3
neutral impurity	$\sigma \propto T^{0.75}\exp(-E_i/2k_BT)$	151±4

$$N_C = \frac{2(2\pi m_0 k_B T)^{3/2}}{h^3} \quad (2)$$

where m_0 is the effective electron mass in the conduction band, which equals 0.48 times the static electron mass,[34] and h is Planck's constant.

The temperature dependence of electron mobility ($\mu = \mu(T)$) varies with different scattering mechanisms. The three most important mechanisms in AlN between 180 and 300 K were considered here: acoustic deformation potential scattering, Coulomb scattering, and neutral impurity scattering, which yield $\mu - T$ dependence: $\mu \propto T^{-1.5}$, $\mu \propto T^{1.5}$, and $\mu \propto T^0$, respectively.[32] Their $\sigma - T$ relationships and corresponding calculated E_i values from fitting the $\sigma - T$ curves are listed in Table 1.

All of the above three relationships give quite satisfactory fitting results (Figure 9b). The resistivity of the AlN nanoneedle consisted of the contribution from all three mechanisms. Therefore, the excitation energy of the impurity in the AlN nanoneedle should lie in between the maxium and minimum value obtained in Table 1, that is, 83 meV $\leq E_i \leq$ 223 meV, which is in agreement with previous results of *n*-type Si-doped AlN,[30–32] but significantly different from the typical value of another effective impurity (Mg) in AlN.[1,35] Therefore, it was very likely that silicon was the impurity repsonsible for the electrical properties.

We also estimate the concentration of Si impurity using room temperature data. Assuming that there was only one impurity level and that there was no compensation effect, the Si concentration (N_D) can be calculated by solving eq 1. An E_i value of 250 meV[32] was adopted according to literature. In previous reports, the electron mobility of Si-doped AlN thin films vary from less that 1 to about 200 $cm^2\ V^{-1}\ s^{-1}$.[31,32] A low mobility value of 0.1 $cm^2\ V^{-1}\ s^{-1}$ was used to get the maximum Si concentration required for conductivity. The measured conductivity could be achieved at a Si concentration as low as 10^{15} cm^{-3}. This value should be smaller if a larger mobility value was used in estimation. The silicon concentration incorporated into the AlN nanoneedles was beyond the detection limit of EDS. However, the silicon substrates were involved in the reaction quite significantly as indicated by the polycrystalline Si XRD pattern. It was reasonable to speculate that the amount of doped Si was sufficient to achieve the value required for the measured conductivity and was responsible for the observed electrical conductance behavior. More detailed electrical properties of AlN 1D nanostructures were under investigation.

CONCLUSIONS

We demonstrated that [0001] oriented AlN 1D nanostructures with manifold morphologies could be selectively obtained by controlling temperature and NH_3 flow in an Al−NH_3 CVD system. A surface diffusion-controlled mechanism was proposed to interpret morphology evolution, which was expected to shed light on the growth of other wurtzite 1D nanostructures. In addition, the electrical properties of a single AlN nanoneedle sample was first studied, in which *n*-type semiconductor behaviors were found, suggesting the potential applications of AlN 1D nanostructures in electronic/optoelectronic nanodevices.

EXPERIMENTAL SECTION

The experiment setup for material preparation consisted of a quartz tube (2.5 cm in diameter) mounted in a tube furnace, a pumping system, and a gas flow control system. Al powder (0.3 g) (99.9%) was loaded in an alumina boat, spreading a range of 2.5 cm. Single side polished Si (100) wafers (10 mm × 5 mm) with a 100 nm oxide layer were served as substrates and placed right above the aluminum powder with a gap of 5 mm. No catalyst was deposited on the substrates. The system was evacuated to 0.6 Pa and was flushed with pure Ar several times to remove oxygen and moisture. The furnace was heated under an Ar flow of 50 sccm (stand cubic centimeter per minute) at 20 °C/min. After reaching the desired temperature, a certain amount of NH_3 was introduced. In our investigations, the temperature and NH_3 flow varied from 950 to 1050 °C and 1 to 25 sccm, respectively. The system was maintained at constant temperature and gas flow for 3 h. After that, NH_3 flow was cut off, and the system was cooled down to room temperature under 50 sccm Ar. Deposition was found on both sides of the silicon substrates. The deposits on the polished side were characterized by X-ray diffraction (XRD, Rigaku D/max-200 diffractometer, Cu Kα), scanning electron microscopy (SEM, Hitachi S4800), and high resolution transmission electron microscopy (HRTEM, Tecani F30) equipped with an energy dispersive spectroscopy (EDS) detector. Most samples discussed in this article were collected on the upper side of the substrates with only one exception. Electrical properties of AlN nanoneedles were measured on a Keithley 6430 sourcemeter and a home-built measurement platform whose background noise is mostly smaller than 0.1 pA.

Acknowledgment. This work was supported by NSFC (Nos. 20221101, 10335040, and 20671004), MOST of China (No. 2006AA05Z130), and MOE of China (No. 707002). We thank Professor Dapeng Yu from College of Physics, Peking University for assisting with the electrical properties measurements.

Supporting Information Available: More SEM images of the nanoneedles and branched nanoneedles and a brief discussion of the effect of silicon substrates. This material is available free of charge via the Internet at http://pubs.acs.org.

REFERENCES AND NOTES

1. Taniyasu, Y.; Kasu, M.; Makimoto, T. An Aluminium Nitride Light-Emitting Diod with a Wavelength of 210 Nanometres. *Nature* **2006**, *441*, 325–328.
2. Taniyasu, Y.; Kasu, M.; Makimoto, T. Field Emission Properties of Heavily Si-Doped AlN in Triode-Type Display Structure. *Appl. Phys. Lett.* **2004**, *84*, 2115–2117.
3. Tsubouchi, K.; Mikoshiba, N. Zero-Temperature-Coefficient SAW Devices on AlN Epitaxial Films. *IEEE Trans. Sonics Ultrason.* **1985**, *32*, 634–644.

4. Lu, H.; Schaff, W. J.; Hwang, J.; Wu, H.; Koley, G.; Eastman, L. F. Effect of an AlN Buffer Layer on the Epitaxial Growth of InN by Molecular-Beam Epitaxy. *Appl. Phys. Lett.* **2001**, *79*, 1489–1491.
5. Xia, Y. N.; Yang, P. D.; Sun, Y. G.; Wu, Y. Y.; Mayers, B.; Gates, B.; Yin, Y. D.; Kim, F.; Yan, Y. Q. One-Dimensional Nanostructures: Synthesis, Characterization, and Applications. *Adv. Mater.* **2003**, *15*, 353–389.
6. Zhang, Y. J.; Liu, J.; He, R. R.; Zhang, Q.; Zhang, X. Z.; Zhu, J. Synthesis of Aluminum Nitride Nanowires from Carbon Nanotubes. *Chem. Mater.* **2001**, *13*, 3899–3905.
7. Wu, Q.; Hu, Z.; Wang, X. Z.; Chen, Y.; Lu, Y. N. Synthesis and Optical Characterization of Aluminum Nitride Nanobelts. *J. Phys. Chem. B* **2003**, *107*, 9726–9729.
8. Tang, Y. B.; Cong, H. T.; Wang, Z. M.; Cheng, H. M. Synthesis of Rectangular Cross-section AlN Nanofibers by Chemical Vapor Deposition. *Chem. Phys. Lett.* **2005**, *416*, 171–175.
9. Liu, C.; Hu, Z.; Wu, Q.; Wang, X. Z.; Chen, Y.; Sang, H.; Zhu, J. M.; Deng, S. Z.; Xu, N. S. Vapor-Solid Growth and Characterization of Aluminum Nitride Nanocones. *J. Am. Chem. Soc.* **2005**, *127*, 1318–1322.
10. Zhao, Q.; Zhang, H. Z.; Xu, X. Y.; Wang, Z.; Xu, J.; Yu, D. P.; Li, G. H.; Su, F. H. Optical Properties of Highly Ordered AlN Nanowire Arrays Grown on Sapphire Substrate. *Appl. Phys. Lett.* **2005**, *86*, 193101.
11. Shi, S. C.; Chen, C. F.; Chattopadhyay, S.; Lan, Z. H.; Chen, K. H.; Chen, L. C. Growth of Single-Crystalline Wurtzite Aluminum Nitride Nanotips with a Self-Selective Apex Angle. *Adv. Funct. Mater.* **2005**, *15*, 781–786.
12. Wu, Q.; Hu, Z.; Wang, X. Z.; Lu, Y. N.; Chen, X.; Xu, H.; Chen, Y. Synthesis and Characterization of Faceted Hexagonal Aluminum Nitride Nanotubes. *J. Am. Chem. Soc.* **2003**, *125*, 10176–10177.
13. Tang, Y. B.; Cong, H. T.; Chen, Z. G.; Cheng, H. M. An Array of Eiffel-Tower-Shape AlN Nanotips and its Field Emission Properties. *Appl. Phys. Lett.* **2005**, *86*, 233104-1–233104-3.
14. Zhao, Q.; Xu, J.; Xu, X. Y.; Wang, Z.; Yu, D. P. Field Emission from AlN Nanoneedle Arrays. *Appl. Phys. Lett.* **2004**, *85*, 5331–5333.
15. Tang, Y. B.; Cong, H. T.; Cheng, H. M. Field Emission from Honeycomb-like Network of Vertically Aligned AlN Nanoplatelets. *Appl. Phys. Lett.* **2006**, *89*, 093113-1–093113-3.
16. Shi, S. C.; Chen, C. F.; Chattopadhyay, S.; Chen, K. H.; Chen, L. C. Field Emission from Quasi-Aligned Aluminum Nitride Nanotips. *Appl. Phys. Lett.* **2005**, *87*, 073109-1–073109-3.
17. Yin, L. W.; Bando, Y.; Zhu, Y. C.; Li, M. S.; Li, Y. B.; Golberg, D. Growth and Field Emission of Hierarchical Single-Crystalline Wurtzite AlN Nanoarchitectures. *Adv. Mater.* **2005**, *17*, 110–114.
18. Northrup, J. E.; DiFelice, R.; Neugebauer, J. Atomic Structure and Stability of AlN(0001) and (0001) Surfaces. *Phys. Rev. B* **1997**, *55*, 13878–13883.
19. Koblmueller, G.; Averbeck, R.; Geelhaar, L.; Riechert, H.; Hosler, W.; Pongratz, P. Growth Diagram and Morphologies of AlN Thin Films Grown by Molecular Beam Epitaxy. *J. Appl. Phys.* **2003**, *93*, 9591–9596.
20. Mula, G.; Adelmann, C.; Moehl, S.; Oullier, J.; Daudin, B. Surfactant Effect of Gallium During Molecular-Beam Epitaxy of GaN on AlN (0001). *Phys. Rev. B* **2001**, *64*, 195406-1–195406-12.
21. Cao, Y. G.; Xie, M. H.; Liu, Y.; Ng, Y. F.; Wu, H. S.; Tong, S. Y. In N Island Shape and its Dependence on Growth Condition of Molecular-Beam Epitaxy. *Appl. Phys. Lett.* **2003**, *83*, 5157–5159.
22. Shi, S. C.; Chattopadhyay, S.; Chen, C. F.; Chen, K. H.; Chen, L. C. Structural Evolution of AlN Nano-Structures: Nanotips and Nanorods. *Chem. Phys. Lett.* **2006**, *418*, 152–157.
23. Zheng, J.; Song, X. B.; Yu, B.; Li, X. G. Asymmetrical AlN Nanopyramids Induced by Polar Surfaces. *Appl. Phys. Lett.* **2007**, *90*, 3121–3125.
24. Nam, C. Y.; Tham, D.; Fischer, J. E. Effect of the Polar Surface on GaN Nanostructure Morphology and Growth Orientation. *Appl. Phys. Lett.* **2004**, *85*, 5676–5678.
25. Ehrlich, G.; Hudda, F. G. Atomic View of Surface Self-Diffusion: Tungsten on Tungsten. *J. Chem. Phys.* **1966**, *44*, 1039–1049.
26. Schwoebel, R. L.; Shipsey, E. J. Step Motion on Crystal Surfaces. *J. Appl. Phys.* **1966**, *37*, 3682–3686.
27. Mensah, S. L.; Kayastha, V. K.; Ivanov, I. N.; Geohegan, D. B.; Yap, Y. K. Formation of Single Crystalline ZnO Nanotubes without Catalysts and Templates. *Appl. Phys. Lett.* **2007 90**, 113108-1–113108-3.
28. Mattila, T.; Nieminen, R. M. Ab Initio Study of Oxygen Point Defects in GaAs, GaN, and AlN. *Phys. Rev. B* **1996**, *54*, 16676–16682.
29. Park, C. H.; Chadi, D. J. Stability of Deep Donor and Acceptor Centers in GaN, AlN, and BN. *Phys. Rev. B* **1997**, *55*, 12995–13001.
30. Hermann, M.; Furtmayr, F.; Bergmaier, A.; Dollinger, G.; Stutzmann, M.; Eickhoff, M. Highly Si-Doped AlN Grown by Plasma-Assisted Molecular-Beam Epitaxy. *Appl. Phys. Lett.* **2005**, *86*, 192108-1–192108-3.
31. Taniyasu, Y.; Kasu, M.; Kobayashi, N. Intentional Control of n-type Conduction for Si-doped AlN and AlxGa1-xN (0.42 $<= x <$ 1). *Appl. Phys. Lett.* **2002**, *81*, 1255–1257.
32. Taniyasu, Y.; Kasu, M.; Makimoto, T. Electrical Conduction Properties of n-type Si-doped AlN with High Electron Mobility ($>$ 100 cm(2) V-1 s($-$1)). *Appl. Phys. Lett.* **2004**, *85*, 4672–4674.
33. Seeger, K., *Semiconductor Physics, An Introduction*. 3rd ed.; Springer-Verlag: New York, 1985.
34. Chin, V. W. L.; Tansley, T. L.; Osotchan, T. Electron Mobilities in Gallium, Indium, and Aluminum Nitrides. *J. Appl. Phys.* **1994**, *75*, 7365–7372.
35. Nam, K. B.; Nakarmi; M. L.; Li, J.; Lin, J. Y.; Jiang, H. X. Mg Acceptor Level in AlN Probed by Deep Ultraviolet Photoluminescence. *Appl. Phys. Lett.* **2003**, *83*, 878–880.